

Control of wind-induced motion in high-rise buildings with hybrid TM/MR dampers

Aly Mousaad Aly*

*Department of Civil and Environmental Engineering, Louisiana State University,
3513D Patrick Taylor Hall, Baton Rouge, LA 70803, USA*

(Received June 8, 2015, Revised October 16, 2015, Accepted October 20, 2015)

Abstract. In recent years, high-rise buildings received a renewed interest as a means by which technical and economic advantages can be achieved, especially in areas of high population density. Taller and taller buildings are being built worldwide. These types of buildings present an asset and typically are built not to fail under wind loadings. The increase in a building's height results in increased flexibility, which can lead to significant vibrations, especially at top floors. Such oscillations can magnify the overall loads and can be annoying to the top floors' occupants. This paper shows that increased stiffness in high-rise buildings may not be a feasible solution and may not be used for the design for comfort and serviceability. High-rise buildings are unique, and a vibration control system for a certain building may not be suitable for another. Even for the same building, its behavior in the two lateral directions can be different. For this reason, the current study addresses the application of hybrid tuned mass and magneto-rheological (TM/MR) dampers that can work for such types of buildings. The proposed control scheme shows its effectiveness in reducing floors' accelerations for both comfort and serviceability concerns. Also, a dissipative analysis carried out shows that the MR dampers are working within the possible range of optimum performance. In addition, the design loads are dramatically reduced, creating more resilient and sustainable buildings. The purpose of this paper is to stimulate, shape, and communicate ideas for emerging control technologies that are essential for solving wind related problems in high-rise buildings, with the objective to build the more resilient and sustainable infrastructure and to optimally retrofit existing structures.

Keywords: high-rise buildings; wind-induced vibration; robust control; tuned mass damper; magneto-rheological damper; semi-active control; dissipative analysis

1. Introduction

1.1 Renewed interest in high-rise buildings

4000 years ago, the Egyptians built the tallest Pyramid of Giza, which was considered the highest and the first construction built based on scientific calculations. In modern times, there have been renewed interest in constructing taller and taller buildings (Pelli *et al.* 1997). Early in 1930, the 282.5 m Bank of Manhattan tower was built in New York City. Within a span of two years, the 319 m Chrysler Building and the 381 m Empire State Building (in 1931) were built. In 2003, the

*Corresponding author, Assistant Professor, E-mail: aly@LSU.edu

509 m Taipei 101 became the world's tallest building after the 452 m Petronas Towers in Kuala Lumpur. Currently the 828 m Burj Khalifa in Dubai is the tallest building in the world (CTBUH, 2015). However, this race to build taller and taller towers seems to continue, probably in 2018 the Kingdom Tower in Jeddah, will be significantly higher, with a proposed height of at least 1,000 m. An important question is raised, why the world is going towards building taller and taller towers? Is there any advantage in these high-rise buildings? From an occupational perspective, some people may think that inhabitants living in high-rise apartments are lonely and unhappy; while others may ponder that it is advantageous to stay in high-rise buildings. High-rise buildings satisfy the demand of rentals in cities to an extent; they are excellent places for a short stay as the prices of apartments are low compared to individual homes in cities. Occupants can enjoy the facilities and high living standards which are often offered by the urban life, such as, business centers, hospitals, transportation networks, recreational facilities, etc. High-rise apartment buildings are typically built in desirable urban locations that yield a variety of lifestyle features and amenities, including the proximity of shopping centers, nightlife, public transportation, doormen, fitness centers, controlled entry, security systems, on-site maintenance, guest housing, and morning coffee. Furthermore, living in a high-rise building may provide a real sense of community. For instance, large buildings host regular resident events or fitness classes that provide an opportunity for inhabitants to know their neighbors. High-rise apartments typically result in lower utility costs, due to construction standards and practices (Anthony and Stainer 1988, Jin *et al.* 2013). Heating and cooling systems can be more efficient in high-rise buildings, compared to individual homes. Also, on high-rise buildings, wind has potential beneficial effects that can be used for extracting wind energy using wind turbines, as their efficiency can be significantly improved compared with ground level (Irwin *et al.* 2008, Khayrullina *et al.* 2013). In any case, due to the increasing demand of housing and decreasing availability of land, high-rises are now escalating worldwide, especially in cities.

1.2 Wind effects on buildings

It is true that we cannot see wind, but we can see its effects. For instance, seeing the leaves on a tree wobbling will give an indication that the weather is windy. Apart from its benefits in the field of wind energy and air pollution dispersion (moderate wind), in structural engineering, strong and extreme wind events can have devastating effects on the infrastructure. Extreme winds may cause damage to low-rise buildings in a form of window damage, roof loss, or even complete collapse of wooden structures. In tall buildings, wind can act as a friend. For instance, wind energy harvesting is favorable on high-rise buildings as per smooth and attractive wind flow that can be available on daily basis (Khayrullina *et al.* 2013). However, both cladding loads and the dynamics of the structure become a concern (Irwin *et al.* 2008). Even if the design can satisfy strength requirements, high-rise buildings are usually flexible, as per the use of high-strength lightweight materials, longer floor spans, and slender framing systems. Such flexibility leads to unfavorable vibrations that may affect the structural serviceability and occupants' comfort when subjected to dynamic loads, for instance brought by the wind. Wind-induced vibrations may cause annoyance to the occupants (especially in the upper floors), impaired function of instruments, or structural damage. Because of this, wind loads and the associated wind responses are a governing factor in the design of many high-rise buildings. Consequently, wind-induced vibrations should be controlled not to lead to serious structural damage, potential failure, or affected serviceability.

1.3 Vibration control

Vibration control of structures is an area of current research that looks promising to improve resilience, serviceability, and sustainability of the infrastructure under dynamic loads. Structural control can be achieved by various means, such as modifying rigidities, masses, or damping, and by providing passive or active counter forces. These counter forces can be provided by passive, active, or semi-active control systems (Housner *et al.* 1997). The advantages and limitations of each scheme have been documented and the choice of which approach to use depends largely on the type of the structure, its location, the nature of the dynamic load, project commissioning, and engineering preference.

1.3.1 Passive control systems

A passive control scheme does not need a power supply to function, which is an advantage, for instance, in case of power failure. Several examples of passive control systems are common. Viscous dampers have been used in civil structures and tall buildings for wind-induced response reduction (Hart *et al.* 2010, Taylor 2010), however, in very slender buildings it can be challenging to install these devices. Aly *et al.* (2011a) presented an outer bracing system to control the response of a very slender building. Nevertheless, for buildings where there is no sufficient space for the outer bracing, an alternative control system is required.

One of the most common devices for the control of tall buildings is the tuned mass damper (TMD). TMDs have been implemented in tall buildings and towers to reduce wind-induced vibrations, for example, the Citicorp Center Office Building in New York City, the Chiba Port Tower in Japan, the Centrepoint Tower in Sydney, the John Hancock Tower in Boston, the Taipei 101 Tower in Taiwan and the Milad Tower in Iran (Ghorbani-Tanha *et al.* 2009). A classical TMD consists of a small damped spring-mass system connected to a primary structure (Fig. 1). Typically the frequency of the TMD is tuned to that of the primary structure, and when excited the TMD will resonate and hence dissipate the input energy. By optimally selecting the damping and the tuning frequency of the TMD, maximum response reduction in the primary structure can be attained. Nevertheless, the tuning frequency of the TMD depends on the uncertain estimate of the natural frequency of the primary structure, which makes the design of a robust TMD challenging. Uncertainties in the frequency of the primary structure may exist as per changing ambient conditions, such as, wind speed (aeroelastic effects, Gu and Peng 2002), temperature, relative humidity, building occupancy, localized damage, among other factors (Lee and Yun 2006, Yuen and Kuok 2010a, b, Clinton *et al.* 2006, Liu and DeWolf 2007). In any case, passive control systems have limited ability to adapt to structural changes and loading conditions. To overcome these shortcomings, active and semi-active control schemes can be used.

1.3.2 Active control schemes

An active control scheme uses a power source to drive actuator(s) that apply forces to a primary structure in a prescribed manner. For example, by introducing an active force to act between the structure and the TMD (active tuned mass damper (ATMD)) both the effectiveness and robustness of the TMD can be enhanced. These forces can be used to both add and dissipate energy in the structure. Many researchers have carried out investigations on the design techniques, control strategies, and performance of the ATMD and promising results are documented in the literature (Soong 1990, Dyke *et al.* 1996, Housner *et al.* 1997, Gu and Peng 2002, Li *et al.* 2010, Lu *et al.* 2012). The results presented by Gu and Peng (2002), from an experimental study of an actively

controlled tall building subjected to wind loads, show that the cross-wind vibration control efficiency is higher than that of the along-wind vibration control. On one hand, this is a valuable conclusion as wind loads usually produce higher structural responses in the cross-wind direction, compared to the along-wind direction. On the other hand, ATMDs are large, heavy, and take up valuable space in a building. Moreover, they present an additional cost to a constructional project, require external power, routine maintenance, high-performance digital signal processors and bulky power amplifiers to drive actuators, and can become unstable. To alleviate these problems, semi-active and hybrid control schemes were explored with different combinations and configurations to improve the efficacy of the control system (Park and Ok 2015).

1.3.3 Semi-active control schemes

Semi-active control techniques combine active and passive control schemes and attempt to offer the advantages of both systems with better performance. For example, variable orifice dampers, shape memory alloys (Gur *et al.* 2014), magnetorheological (MR) fluid dampers and electrorheological (ER) fluid dampers (Halsey 1992) have the features of a semi-active control system. Due to their low-power requirements and fail safe property, MR dampers have been enjoying renewed interest as an attractive means for protecting civil infrastructure systems against severe earthquake and wind loading (Leitmann 1994, Dyke *et al.* 1996, Spencer *et al.* 1997, Goncalves *et al.* 2006, Metwally *et al.* 2006, Aly *et al.* 2011). Several approaches have been proposed in the literature to control MR dampers (Jansen and Dyke 2000). Similar to viscous dampers, the challenge in using such devices in tall buildings is related to where, in a building, these devices can be installed to work effectively. In tall buildings, it is required that the damper is connected between two points where a significant displacement is expected.

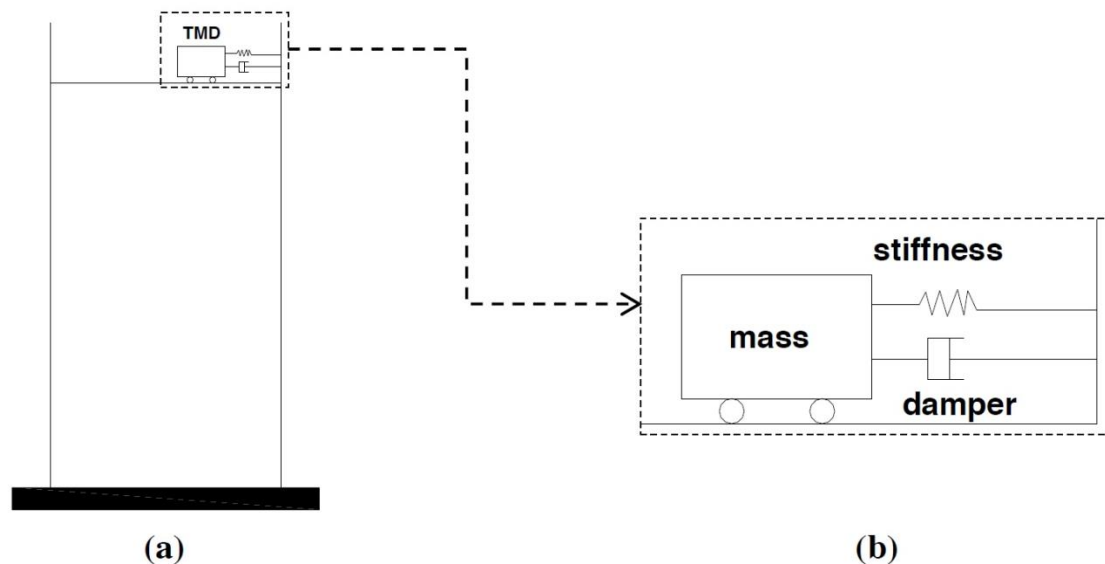


Fig. 1 Schematic of a TMD on a top of a building (a) with its main components (b)

Unlike short and shear buildings, in which floor rotational angles are very small and there may be a significant inter-story drift under dynamic loads, slender and tall buildings may vibrate like a cantilever. It is worthy to mention that bracing systems have been used for the control of tall buildings under wind loads by several researchers. For instance, Kim *et al.* (2014) presents a wind-induced vibration control of tall buildings using hybrid buckling-restrained braces. The system showed significant effectiveness in vibration suppression. However, cantilever-like behavior of buildings makes it very difficult to have an effective internal bracing system (inter-story shear drift is usually not sufficient for a damper to work effectively).

1.4 Paper layout

The current study addresses the application of a hybrid TM/MR damper for response reduction in high-rise buildings under wind loads. The proposed control system combines the advantages of both active and passive control schemes and alleviates the challenge of the use of viscous and smart dampers in slender buildings. The paper is organized as follows. Section 2 presents an application case study building that is instructive. The building has unequal aspect ratios in the two lateral directions, which required the use of two different control systems in each direction. In Section 3, the dynamic responses of the building, uncontrolled and with stiffness increase, are obtained. The purpose of stiffness increase is to investigate its effect on the response, as a direct passive control option. Since the stiffness increase approach is proved to be ineffective, in Section 4, a TMD is proposed to control the response of the building in one lateral direction, with an attempt to control the response in the other direction. While the TMD is shown to be effective in one direction, it is ineffective in the other direction, accordingly in Section 5 MR dampers with lever mechanism are proposed. To further investigate the performance of the proposed control system, a dissipative analysis is presented in Section 6. Finally, the conclusions drawn from the current study are summarized in Section 7.

2. An application case study

To show the applicability and the motivations of using the proposed hybrid TM/MR dampers control system in high-rise buildings, a case study building subjected to multi-directional wind loads is investigated. In this section, the mathematical modelling of the building is presented, along with the wind excitation loads.

2.1 Building's model

A numerical model representative of a full-scale concrete high-rise building is used in the current study. The building has a height of 221.3 m aboveground and a rectangular cross-section of $B/D = 2.56$ (B : chord length, D : thickness). The aspect ratio is nearly 10, which makes it very slender and sensitive to strong winds. The overall building's mass is about 1.4×10^5 tons. The structure has 50 stories above ground level. There are four underground stories. A finite element (FE) model of the full-scale building was built using Midas Gen ver. 7.2.1 (Midas 2015). Thanks to the refinement of the calculation models it is possible to analyse the behaviour of all of the competitive elements of the same member, which allow for considering the effective contribution to the total rigidity of the system supplied from every elementary member. In building up the

model, the following finite elements were used: (1) plate element: to model the slaps of the floors; (2) beam element: to model beams and pillars; and (3) truss element: for modelling steel bars. The three-dimensional FE model represents the whole building including the underground part. The first six modes of vibration obtained by finite element (FE) modeling are shown in Fig. 2. The first six natural frequencies are: 0.122 Hz, 0.135 Hz, 0.461 Hz, 0.647 Hz, 1.079 Hz and 1.083 Hz, respectively. As explained later in this subsection, this building behaves in shear in the x-direction and as a cantilever in the y-direction (very slender); further description of the building is provided in Aly (2009).

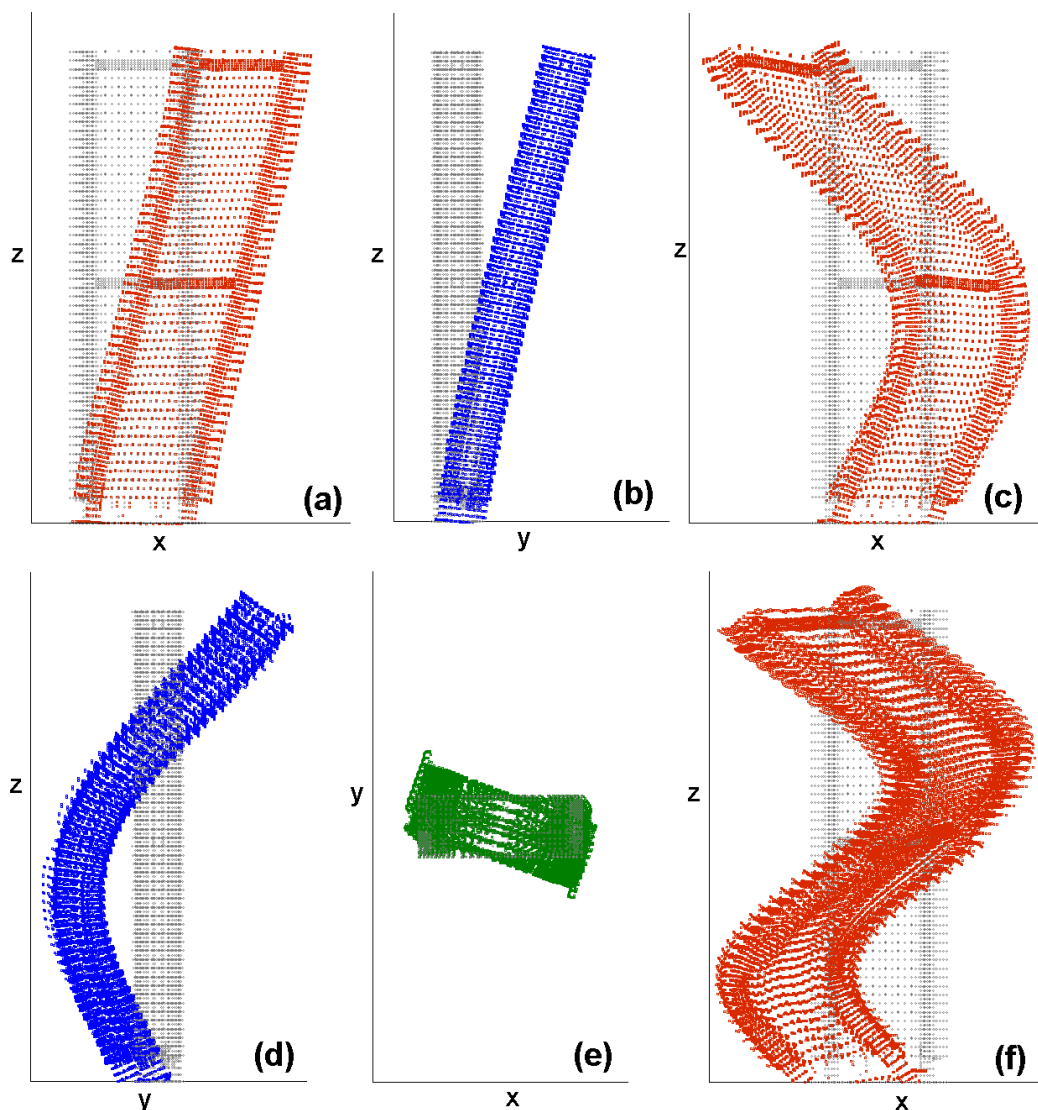


Fig. 2 Mode shapes of the case study building: (a) first mode, (b) second mode, (c) third mode, (d) fourth mode, (e) fifth mode, and (f) sixth mode

While mode shapes and natural frequencies can be obtained by FE modelling, it is difficult to obtain the structural damping in a similar way. This is because, unlike mass and rigidities that are distributed along structural elements, damping is related to friction between joints and some hysteresis in the material and there is no convenient means of refining the predictive capabilities regarding inherent structural damping. Accordingly, there have been some efforts to develop empirical predictive tools for damping estimation based on full-scale observations (Li *et al.* 2002, Satake *et al.* 2003, Smith and Willford 2007). As a result of these efforts, Tamura and Yoshida (2008) presented a damping predictor for tall buildings that is dependent on the response amplitude. The formula for reinforced concrete buildings is given by

$$\zeta = \frac{0.93}{H} + 470 \frac{x_H}{H} - 0.001 \quad (1)$$

where ζ is the first modal damping, x_H is the displacement at the top of the building, and H is the building's height. For $x_H = 0.5$ m and overall building height of about 240 m (including underground stories), the damping factor from the above equation is about 1%. For $x_H = 0.25$ m and 1 m the corresponding damping factors are 0.5% and 2% respectively. However, the damping factor for this building was assumed to be 1%.

Once mode shapes, natural frequencies, and damping factors are known for a high-rise building, its response can be obtained by integrated the time histories of surface wind loads with these physical parameters, for example, by using the pressure integration technique (Aly 2013). However, for control purposes, as the control devices act together with the structure and there is a potential mode shape change due to such interaction, a lumped masses model is necessary. Consequently, a significant amount of effort was spent to create lumped mass models in both x- and y-directions, to account for the fact that mode shapes with the control devices can be different from those without control. In these lumped masses models, the behavior of the structure was a combination of shear and cantilever responses. To permit such technique of modelling, the diagonal drifts between each two adjacent floors was obtained from the lateral mode shapes. For instance, considering the diagonal length between any two arbitrary floors to be L_b , as shown in Fig. 3, this length will be L_b' after deforming in the lateral direction, say by considering the lower mode shape in a certain direction. By doing so, the drifts can be estimated as listed in Table 1. The results show that significant drifts between different sets of two arbitrary floors are obtained in the x-direction, compared to the y-direction. This indicates that the building behaves in y-direction, mostly as a cantilever (notice significant floor rotation (Fig. 3). However, in the x-direction, the building is mostly like a shear building. Using these lumped masses models, the equations of motion were written in a generic form to permit for investigative control studies.

2.2 Equations of motion

The motion of the building in the 3-D (both the two transverse directions and torsion) can be expressed as

$$\mathbf{M}_s \ddot{\mathbf{x}} + \mathbf{C}_s \dot{\mathbf{x}} + \mathbf{K}_s \mathbf{x} = \mathbf{F} + \mathbf{A} \mathbf{f} \quad (2)$$

where $\mathbf{x} = [\mathbf{X} \ \mathbf{Y} \ \mathbf{\Theta}]^T$. The terms $\mathbf{X} = [x_1 \ x_2 \ \dots \ x_n]$ and $\mathbf{Y} = [y_1 \ y_2 \ \dots \ y_n]$ are row vectors of the displacements of the center of mass of each floor in the x- and y-directions, respectively, and $\mathbf{\Theta} = [\theta_1 \ \theta_2 \ \dots \ \theta_n]$ is the vector of the rotations of each floor about the vertical axis (z-axis), while n is

the number of floors. \mathbf{M}_s , \mathbf{K}_s , and \mathbf{C}_s are mass, stiffness, and damping matrices, respectively. The mass matrix \mathbf{M}_s has the following form

$$\mathbf{M}_s = \begin{bmatrix} \mathbf{M} & \mathbf{0} & \mathbf{0} \\ \mathbf{0} & \mathbf{M} & \mathbf{0} \\ \mathbf{0} & \mathbf{0} & \mathbf{I} \end{bmatrix} \quad (3)$$

where $\mathbf{M} = \text{diag}([m_1 \ m_2 \ \dots \ m_n])$ is a diagonal $n \times n$ matrix of lumped masses, and $\mathbf{I} = \text{diag}([I_1 \ I_2 \ \dots \ I_n])$ where I_i is the moment of inertia of the i^{th} floor. The stiffness matrix \mathbf{K}_s is obtained by assuming the stiffness between adjacent floors as a combination of cantilever and shear rigidities. MATLAB (Attaway 2009) codes were written to derive the best stiffness matrix that provides the closest mode shapes to those of the FE model, and almost the same first six natural frequencies. Consequently, the total stiffness matrix \mathbf{K}_s has the form

$$\mathbf{K}_s = \begin{bmatrix} \mathbf{K}_x & 0 & 0 \\ 0 & \mathbf{K}_y & 0 \\ 0 & 0 & \mathbf{K}_\theta \end{bmatrix} \quad (4)$$

where \mathbf{K}_x , \mathbf{K}_y and \mathbf{K}_θ are the stiffness matrices in the transverse directions (x and y) and the torsional direction, respectively. An uncertainty of 10% in the structural stiffness matrix (corresponds to uncertainty in the natural frequency of about $\pm 5\%$) is assumed to further investigate the robustness of the control system. The damping matrix \mathbf{C}_s was obtained by considering the damping value as an equivalent Rayleigh Damping in the form of (Chowdhury and Dasgupta 2003)

$$\mathbf{C}_s = a \mathbf{M}_s + b \mathbf{K}_s \quad (5)$$

in a and b are pre-defined constants. After estimating the damping matrix, the modal damping vector was obtained for all modes and the first six modal damping ratios were assigned to 1% of the critical value. Consequently, the damping matrix was reconstructed using the new modal damping vector. To obtain the damping matrix, \mathbf{C}_s from the modal damping factors, the approach described in Meirovitch (1967) was followed. According to this approach, at normal modes (when the equations of motion are decoupled), the equations of motion for free damped vibration take the form

$$\mathbf{M}_s \ddot{\mathbf{x}} + \mathbf{C}_s \dot{\mathbf{x}} + \mathbf{K}_s \mathbf{x} = 0 \quad (6)$$

where

$$\mathbf{C}_D = [\mathbf{u}\mathbf{u}]^T [\mathbf{C}_s] [\mathbf{u}\mathbf{u}] = 2 \mathbf{M}_s [\omega] [\zeta] \quad (7)$$

in which, $[\mathbf{u}\mathbf{u}]$ is a matrix of orthonormal modes associated with the eigenvalue problem (eigenvectors), $[\omega]$ is a diagonal matrix of undamped natural frequencies and $[\zeta]$ is a diagonal matrix of modal damping factors.

In Eq. (2), the disturbance $\mathbf{F} = [\mathbf{F}_x \ \mathbf{F}_y \ \mathbf{T}]^T$ is a vector of excitation in which \mathbf{F}_x and \mathbf{F}_y are two vectors of horizontal loads acting in the x- and y-directions, respectively, and \mathbf{T} is a vector of

external torsional wind loads; \mathbf{f} is a vector of control forces, where its coefficient matrix $\mathbf{\Lambda}$ is determined by the location of the control devices.

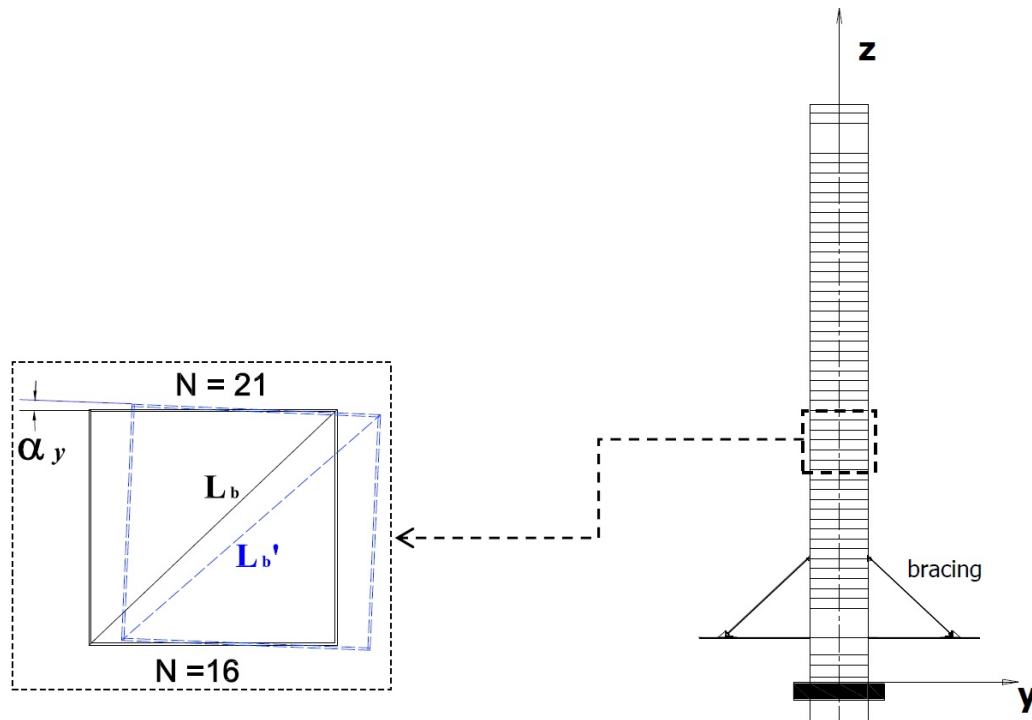


Fig. 3 Diagonal drifts between two arbitrary floors

Table 1 Modal drifts normalized to be 1 m at the top of the building

Floors	Height (m)	x-direction			y-direction		
		L_b (m)	L_b' (m)	δ (m)	L_b (m)	L_b' (m)	δ (m)
Base-0	19.100	48.446	48.459	0.013	28.147	28.150	0.003
0-6	32.800	55.626	55.691	0.065	39.212	39.219	0.007
6-11	20.500	49.449	49.527	0.078	29.808	29.816	0.008
11-16	20.500	49.449	49.537	0.088	29.808	29.816	0.008
16-21	20.500	49.449	49.537	0.088	29.808	29.816	0.008
21-26	20.500	49.449	49.522	0.073	29.808	29.816	0.008
26-31	20.500	49.449	49.525	0.076	29.808	29.816	0.008
31-36	20.500	49.449	49.531	0.082	29.808	29.817	0.009
36-41	20.500	49.449	49.526	0.077	29.808	29.816	0.008
41-46	20.500	49.449	49.514	0.065	29.808	29.814	0.006
46-50	24.300	51.285	51.336	0.051	32.763	32.768	0.005

2.3 Wind loads

The wind load vectors (\mathbf{F}_x , \mathbf{F}_y , and \mathbf{T}) lumped at the position of the floors were obtained from a wind tunnel pressure test conducted on a scaled 1:100 rigid model of the building (Fig. 4). The wind profile represents a typical urban terrain exposure as shown in Fig. 5. The reference mean wind speed was measured at a height of 1 m. Prototype reference mean wind speed is dependent on both the return period and the wind direction angle. The target for the wind profiles was the Eurocode 1 (2004). The turbulence intensities in the longitudinal, lateral and vertical directions are referred to by I_u , I_v and I_w , respectively. The surrounding buildings within a radius of 500 m from the center of the building were also scaled 1:100 and presented on the turning test table (Fig. 4). Pressure taps were distributed on the outer surface of the test model. To allow for sufficient pressure measurements, 400 taps were mapped on the outer surface of the model. Pressure data were acquired at a frequency of 62.5 Hz. Further details about the wind tunnel experiment are given in Aly (2009) and Rosa *et al.* (2012).

Pressure data were integrated on the outer surface of the building to obtain the corresponding time histories of the two directional wind loads at each floor in addition to torsion. For the estimation of the wind loads at each floor, the tributary area for each floor was divided into smaller areas and the time history of the wind loads at each area was found by using the C_p records of the closest pressure tap. Codes were written to estimate the time histories of the wind forces acting at the center of each smaller area. After that, the floor forces in the two directions were obtained from the summation of the forces in each lateral direction. The torsion at each floor is the result of the summation of the force moments about the floor vertical axis.

3. Dynamic response

Following the dynamic modelling of the building, the response can be obtained by directly integrating the equation of motion. Considering the design for serviceability, the maximum floor accelerations should not exceed a certain limit. For this building, the design criterion for serviceability is that the maximum floor acceleration for a wind with a return period of 10 years, should not exceed 20 milli-g as a peak value, and 5.7 milli-g as a standard deviation (STD) value.

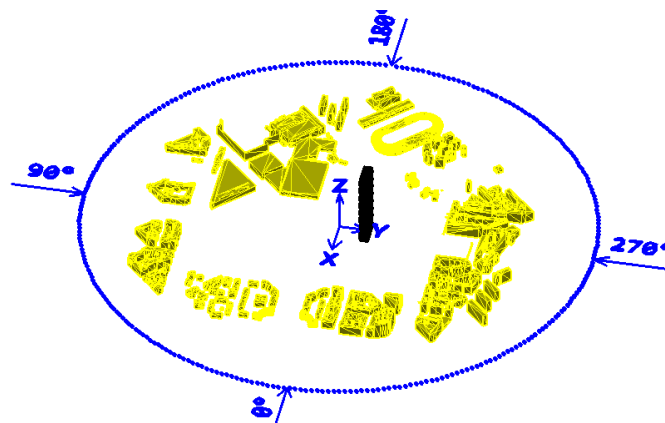


Fig. 4 Schematic showing the orientation of the building with the coordinate system

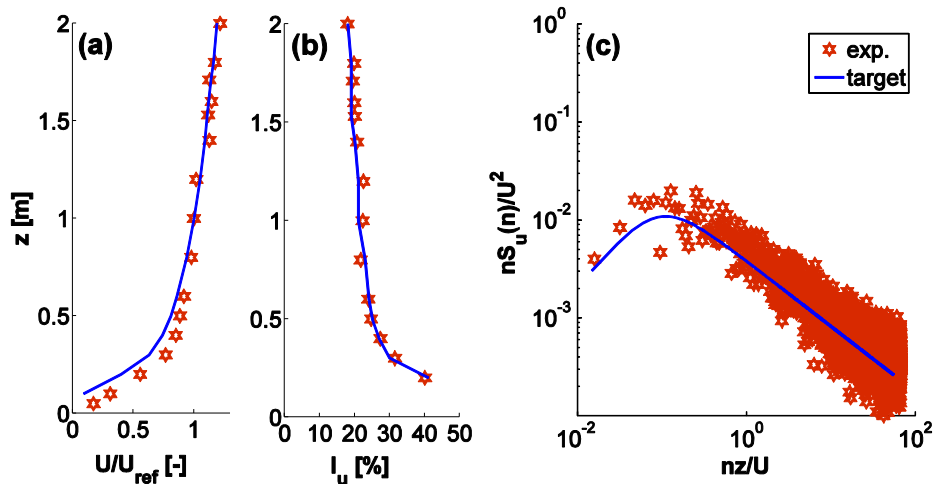


Fig. 5 Flow characteristics: (a) mean wind speed profile, (b) turbulence intensity and (c) velocity spectrum

However, as shown in Figs. 6 and 7 (0% uncontrolled primary structure), the response obtained for the building in the two lateral directions can be higher than the values assigned for the serviceability design. All responses were obtained from the dynamic model of the building under time histories of wind loads obtained from wind tunnel testing at different wind direction angles (α). The stiffness of the dynamic model of building was adapted by considering a multiplication factor to the stiffness matrix in Eq. (4). It is worthy to mention that the prototype wind speed is not the same from all directions; further information about the wind speed directionality is provided in (Aly 2014). The Figs. 6 and 7 show that the cross-wind response of the building in the two lateral directions are significantly higher, compared to the along-wind responses. In any case, the response of a structure may be controlled by modifying rigidities and/or enhancing the inherently low structural damping by implementing external mechanical systems. The first option was investigated by increasing the stiffness of the primary structure by the amounts of 10%, 20%, and 50%. As shown in Figs. 6 and 7, increasing the stiffness of the building by 10% can decrease the acceleration responses in the two directions. A 20% increase in the stiffness may slightly reduce the STD accelerations, without any noticeable reduction in the peak accelerations. By aggressively increasing the stiffness of the primary structure by 50%, the accelerations are slightly reduced in the y-direction. However, the worst STD value in the x-direction was increased, and the peak value was left the same as the uncontrolled structure (0% stiffness increase). To further investigate the stiffness role, Fig. 8 shows the spectra of across-wind loads and the corresponding across-wind building acceleration for the building with 0%, 10%, 20%, and 50% increase in the stiffness (lateral component of response in the y-direction), for a wind direction of 0deg. It is shown that the acceleration response of the top floor, for instance, in the y-direction (without the contribution from torsion), is contributed by lower and higher modes. The amount of increase in the reduced natural frequencies for the corresponding increase in the stiffness of 10%, 20%, and 50% are not significant to expose the building to different excitation forces.

Still the response of the building for 10%, 20%, and 50% stiffness increase significantly higher than the values prescribed by the serviceability requirements. This reveals an important conclusion,

that is, stiffness increase in high-rise buildings is not a feasible solution, and may not be used for the design for comfort and serviceability. Accordingly, the second option that deals with damping enhancement through vibration control will be investigated in the following two sections.

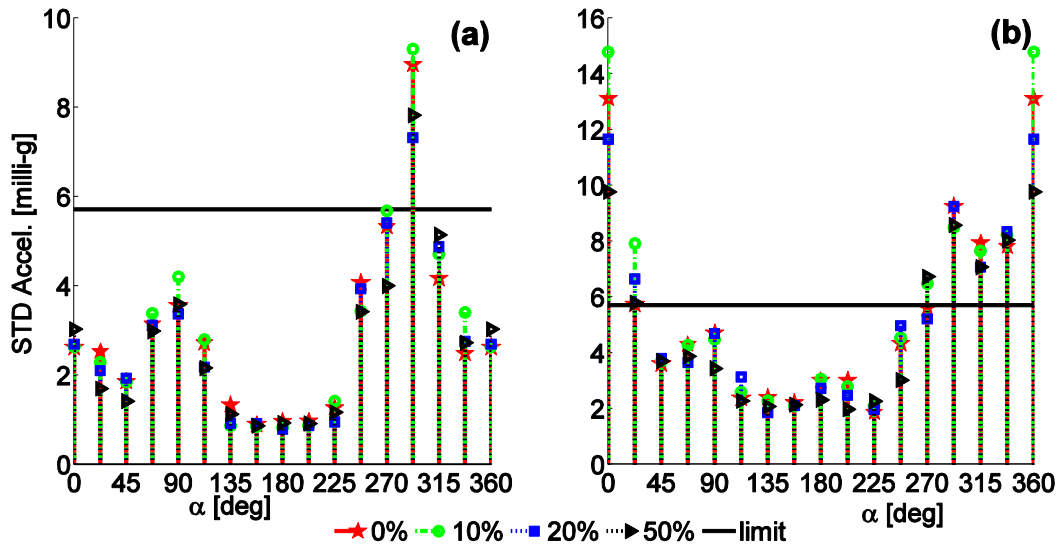


Fig. 6 STD values of the acceleration response for the building with 0%, 10%, 20%, and 50% increase in the stiffness: (a) x-direction, and (b) y-direction

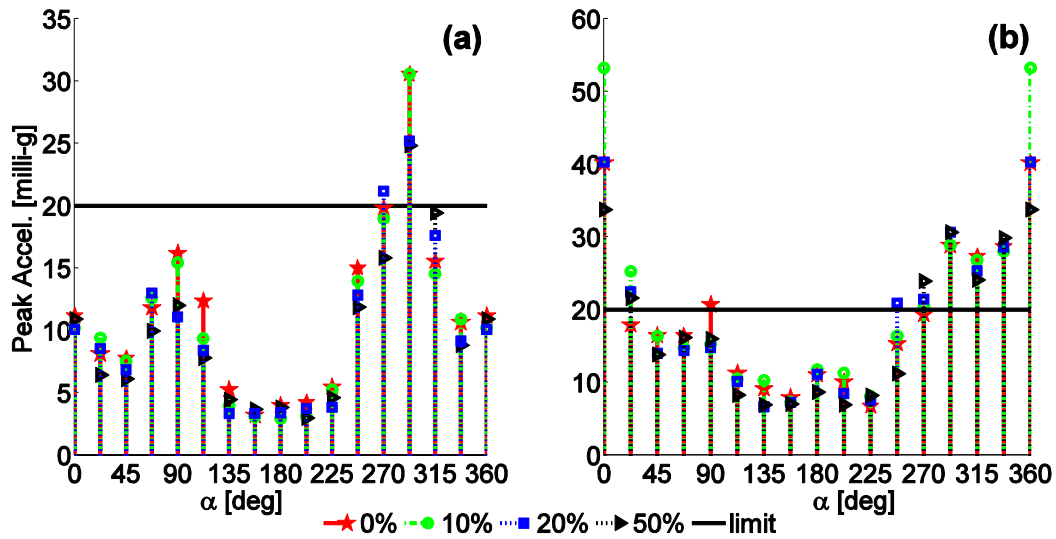


Fig. 7 Peak values of the acceleration response for the building with 0%, 10%, 20%, and 50% increase in the stiffness: (a) x-direction, and (b) y-direction

4. Vibration control by TMD

4.1 Overview

As the building considered in the current study has well separated natural frequencies, and for preliminary TMD design, it can be treated as an equivalent single degree-of-freedom system (SDOF) (see Warburton and Ayorinde 1980). Accordingly, the effect of the TMD can be viewed as being equivalent to changing the damping ratio of the original system from the value $\zeta_1 = C_1/2(K_1M_1)^{0.5}$ to a larger value ζ_e (Simiu and Scanlan 1996). It can be shown that, for a certain tuning frequency ratio, f , the optimal value of the damping coefficient of the TMD is given by (Simiu and Scanlan 1996)

$$\zeta_2^{opt} = \frac{\sqrt{\mu}}{2}; \quad \mu = M_2 / M_1 \quad (8)$$

where μ is the mass ratio (M_1 : primary structure; M_2 : TMD), and the corresponding equivalent damping is

$$\zeta_e^{opt} = \frac{\sqrt{\mu}}{4} + 0.8\zeta_1 > \zeta_1. \quad (9)$$

The optimal tuning frequency f and damping factor ζ_2^{opt} for the TMD, for minimizing displacement, can be obtained from Feng and Mita (1995) as follows

$$f = \frac{\sqrt{1+(\mu/2)}}{(1+\mu)}; \quad \zeta_2^{opt} = \frac{1}{2} \sqrt{(1+\mu)f^4 - \left(\frac{2+\mu}{1+\mu}\right)f^2 + \frac{1}{1-\mu}} \quad (10)$$

In any case, the formulae presented in the literature are mostly obtained for the objective of minimizing the displacement response, and sometimes without clear explanation whether the optimization objective was minimizing wind or earthquake induced response. For this reason, building a mathematical model is advantageous for further investigations, rather than relying on empirical and approximate formulae.

4.2 Numerical optimization under white-noise excitation

For building a reliable mathematical model representative of the TMD with the primary structure, since vibration frequencies and damping modes may vary with wind speed, as it is the case of large and flexible structures, the optimization may be based on an input white-noise excitation. Now the mass, stiffness, and damping of the TMD can be written as functions of the mass ratio μ , the frequency ratio f , the TMD damping factor ζ_2 and the parameters of the primary structure as follows

$$M_2 = \mu M_1; \quad K_2 = \mu M_1 \omega_1^2 f^2; \quad C_2 = 2\mu M_1 \omega_1 f \zeta_2. \quad (11)$$

The equations of motion of the system exposed to white-noise excitation, $w(t)$, can be written as

$$\mathbf{M}_s \ddot{\mathbf{x}}(t) + \mathbf{C}_s \dot{\mathbf{x}}(t) + \mathbf{K}_s \mathbf{x}(t) = \mathbf{G}w(t) \quad (12)$$

where the mass (\mathbf{M}_s), stiffness (\mathbf{K}_s) and damping (\mathbf{C}_s) matrices are characteristic of the primary structure, written as

$$\mathbf{M}_s = M_1 \begin{bmatrix} 1 & 0 \\ 0 & \mu \end{bmatrix}; \mathbf{K}_s = M_1 \omega_1^2 \begin{bmatrix} 1 + \mu f^2 & -\mu f^2 \\ -\mu_1 f^2 & \mu f^2 \end{bmatrix}; \mathbf{C}_s = M_1 \omega_1 \begin{bmatrix} 2\zeta_1 + 2\mu f \zeta_2 & -2\mu f \zeta_2 \\ -2\mu f \zeta_2 & 2\mu f \zeta_2 \end{bmatrix}. \quad (13)$$

In Eq. (12) $\mathbf{x}(t)$ is a vector of displacements, $w(t)$ is the external excitation, \mathbf{G} is the corresponding loading matrix. This system of equations system can be transformed into a first-order time invariant linear system as follows

$$\dot{\mathbf{z}}(t) = \mathbf{A}\mathbf{z}(t) + \mathbf{B}w(t); \quad \mathbf{Y}(t) = \mathbf{C}\mathbf{z}(t) + \mathbf{D}w(t) \quad (14)$$

where $\mathbf{z}(t)$ are the states of the system, $[\mathbf{A}, \mathbf{B}, \mathbf{C}, \text{ and } \mathbf{D}]$ are the associated state-space matrices, and $\mathbf{Y}(t)$ is a vector of desired outputs, which is selected to include displacements and accelerations of the primary system and the inertial mass of the TMD.

Since the excitation $w(t)$ is a stationary white-noise, the time derivative of the covariance matrix of the states $E[\mathbf{z}\mathbf{z}^T]$ is set equal to zero

$$\frac{d}{dt}(E[\mathbf{z}\mathbf{z}^T]) = E[\dot{\mathbf{z}}\mathbf{z}^T + \mathbf{z}\dot{\mathbf{z}}^T] = 0 \quad (15)$$

Substituting Eq. (15) into the first part of Eq. (14) it can be shown that

$$\mathbf{A}E[\mathbf{z}\mathbf{z}^T] + E[\mathbf{z}\mathbf{z}^T]\mathbf{A}^T + \mathbf{B}E[ww^T]\mathbf{B}^T = 0. \quad (16)$$

The disturbance $w(t)$ on the system is a stationary white-noise such that $E[ww^T] = 2\pi S_0$ (Bendat and Piersol 2000). The Eq. (16) can then be rewritten as

$$\mathbf{A}E[\mathbf{z}\mathbf{z}^T] + E[\mathbf{z}\mathbf{z}^T]\mathbf{A}^T = -2\pi S_0 \mathbf{B}\mathbf{B}^T \quad (17)$$

where the covariance matrix of the states, \mathbf{z} , can be determined from Eq. (17) as the solution of the continuous time Lyapunov equation, for example, in MATLAB using the command *lyap.m* (Aly and Christenson 2008, Attaway 2009). The covariance matrix of the output, \mathbf{Y} , is determined from the covariance matrix of the states by employing the second part of Eq. (14), such as,

$$E[\mathbf{Y}\mathbf{Y}^T] = E[(\mathbf{C}\mathbf{z})(\mathbf{C}\mathbf{z})^T] + E[(\mathbf{D}w)(\mathbf{D}w)^T] = \mathbf{C}E[\mathbf{z}\mathbf{z}^T]\mathbf{C}^T + \mathbf{D}E[ww^T]\mathbf{D}^T. \quad (18)$$

Note that the output vector, \mathbf{Y} , gives the responses of the system as standard deviation values.

Relevant numerical techniques are applied to solve the arising optimization problem and to find the optimum parameters of the TMD. For a given mass ratio, μ , one can assume different values of the frequency ratio, f , and for each frequency ratio assuming a range of damping factor ζ_2 of the TMD and estimate the optimum parameters that minimize a certain desired output. Fig. 9 is an example of the numerical optimization conducted to estimate the optimal frequency ratio and damping factor of the TMD for two different mass ratios under wind loads modeled as white-noise. The primary structure is a SDOF system representative of the case study building mentioned in Section 3. The optimization is based on the minimization of the displacement of the primary structure. In this numerical optimization, the responses of the primary structure are normalized,

which means that the response obtained with the TMD when attached to the structure is divided by the corresponding response obtained without the TMD. The optimal values of the frequency ratio and the damping factor of the TMD are written on the subfigures of Fig. 9. It is shown that a TMD with 1% mass ratio can provide a significant reduction in the displacement response of the primary structure. The reduction in the displacement depends very much on the tuning frequency and the damping ratio of the TMD. By increasing the mass ratio from 1% to 5%, the displacement response of the primary structure is reduced. However, the TMD with 5% mass ratio is more robust to the changes in the frequency ratio and the damping factor (the area indicating low normalized response in Fig. 9(b) is larger than that of Fig. 9(a)). By performing the optimization simulations for different mass ratios and obtaining the corresponding optimal tuning frequencies and damping ratios of the TMD based on minimization of displacement or acceleration, one can create a design chart that is helpful in the design process of the TMD (Aly 2014). However, the optimization process does not mean a robust design. For this reason, it can be useful to consider the design of the TMD for a primary structure with stiffness uncertainties and finally choose the TMD parameters that can minimize a response objective for all structural uncertainties (Aly 2014).

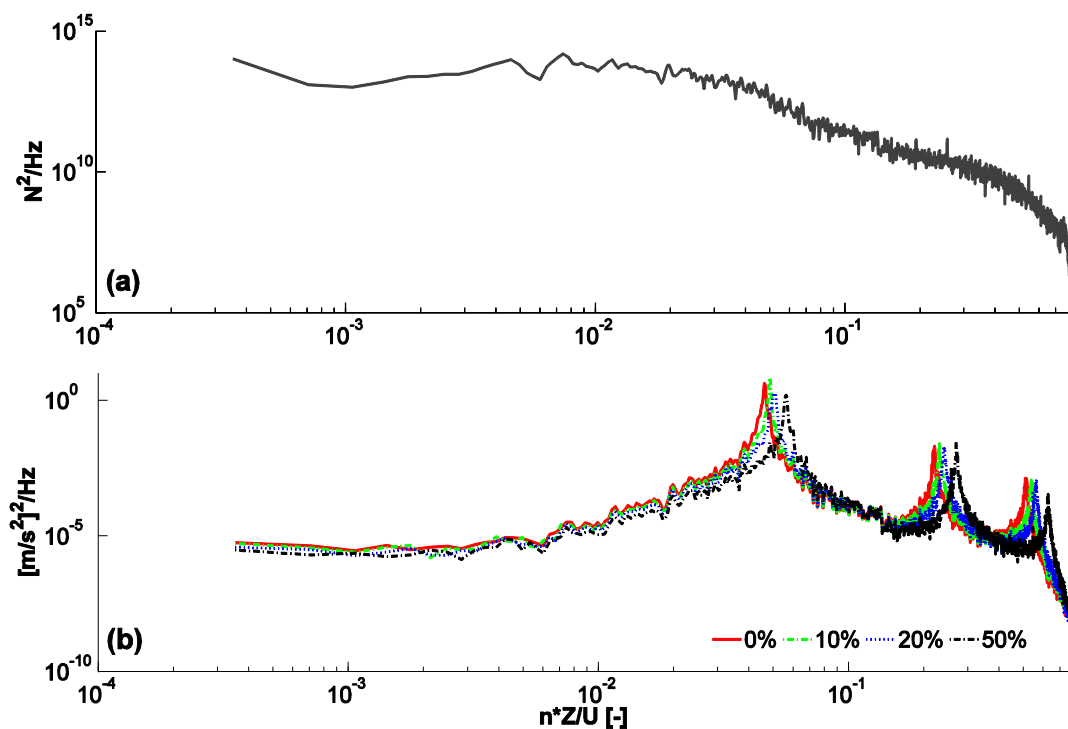


Fig. 8 Spectra of the across-wind loads (a) and the corresponding across-wind acceleration responses (b) for the building with 0%, 10%, 20%, and 50% increase in the stiffness (lateral component of response in the y-direction), for a wind direction of 0deg

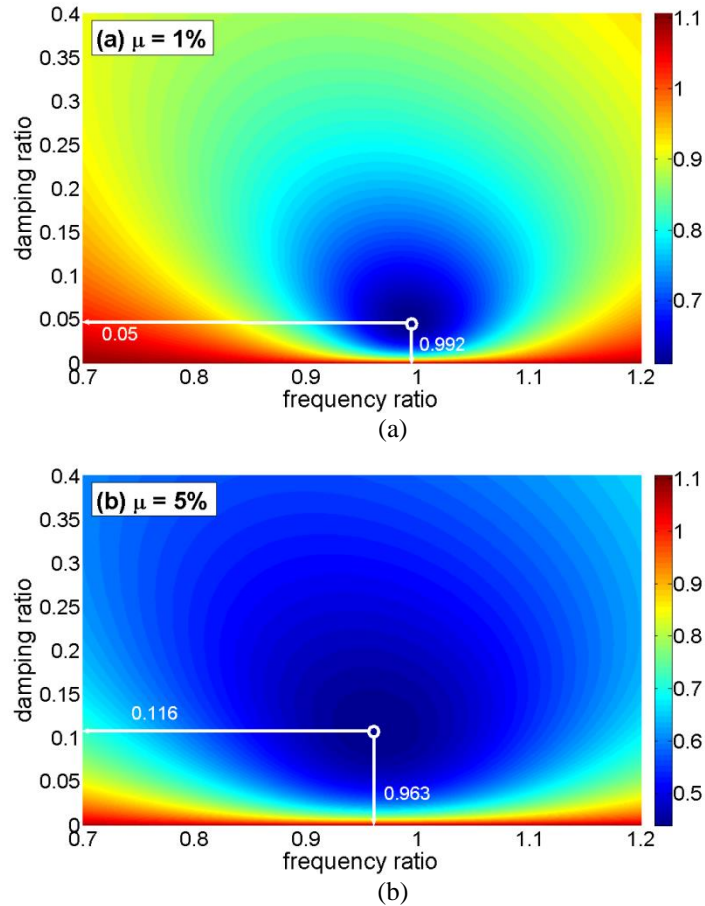


Fig. 9 Effect of changing the frequency and the damping ratios of the TMD on the normalized displacement of the primary structure, for a TMD with: (a) 1%, and (b) 5% mass ratio

4.3 Controlled response in the X-direction

Making use of the optimal parameters obtained from the numerical study, and for a 10% stiffness uncertainty, by iteration, the TMD with 2% mass ratio was chosen for response reduction in the x-direction. Fig. 10 shows the controlled (with TMD) and uncontrolled acceleration responses of the building in the x-direction under wind loads with different direction angles. For comfort concerns, mean wind speed that corresponds to a return of 10 years is considered. The controlled and uncontrolled responses of the building were evaluated by simulations. In the Fig. 10, “Unc.” refers to the uncontrolled acceleration response of the building (without TMD) while “TMD” refers to the acceleration response of the building with TMD. Standard deviation (STD) and peak values of the acceleration response were calculated for all floors of the building, and the maximum value was considered for the serviceability design. Uncertainty in the stiffness of the building of $\pm 10\%$ was considered. On Fig. 10, “0% stiff.” refers to the building with the original stiffness, “+10% stiff.” denotes the building with 10% increase in the original stiffness, and “-10%

stiff.” designates the building with 10% reduction in the original stiffness.

Fig. 10 shows that, for wind loads with a return of 10 years, TMD with a mass ratio of 2% (inertial mass of TMD to the generalized mass of the building in the x-direction) can reduce the acceleration response in terms of RMS and peak values lower than the maximum allowable values (RMS acceleration = 5.7 milli-g and peak acceleration = 20 milli-g). TMD is capable of achieving response reduction over all the wind direction angles. The uncertainty in the building’s stiffness indicates that the TMD is robustly designed. All peak accelerations for a 10 years return floors’ period and peak drifts for a 100 years return period in the x-direction, with and without the TMD, are shown in Fig. 11. Fig. 11 shows that the design for both serviceability and safety is achieved.

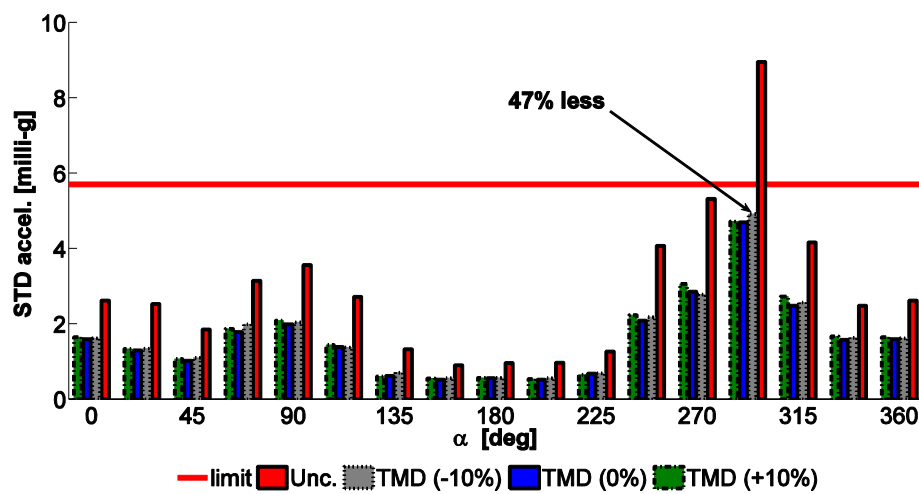


Fig. 10 x-direction acceleration for a 10 years return period

Table 2 Uncontrolled and controlled buildings responses for safety reasons (x-direction at 0°, R = 100 years)

Criteria	Uncontrolled			TMD		
	+0%	+10%	-10%	+0%	+10%	-10%
RMS Disp. (m)	0.2624	0.2636	0.2656	0.1439 (45.16%)	0.1397 (47.00%)	0.1693 (36.26%)
Peak Disp. (m)	0.8594	0.7909	0.7813	0.5356 (37.68%)	0.5164 (34.71%)	0.6073 (22.27%)
Peak Drift (rad)	0.0044	0.0041	0.0042	0.0028 (36.36%)	0.0028 (31.71%)	0.0032 (23.81%)
RMS BS (N)	8.63E+6	9.78E+6	8.16E+6	5.22E+6 (39.46%)	5.56E+6 (43.18%)	5.44E+6 (33.39%)
Peak BS (N)	29.57E+6	31.09E+6	26.57E+6	22.0E+6 (25.77%)	21.0E+6 (32.45%)	21.3E+6 (19.77%)
RMS BM (N.m)	12.72E+8	14.31E+8	11.80E+8	7.14E+8 (43.88%)	7.63E+8 (46.67%)	7.54E+8 (36.16%)
Peak BM (N.m)	43.67E+8	43.26E+8	35.14E+8	26.5E+8 (39.23%)	28.6E+8 (33.98%)	27.4E+8 (22.03%)

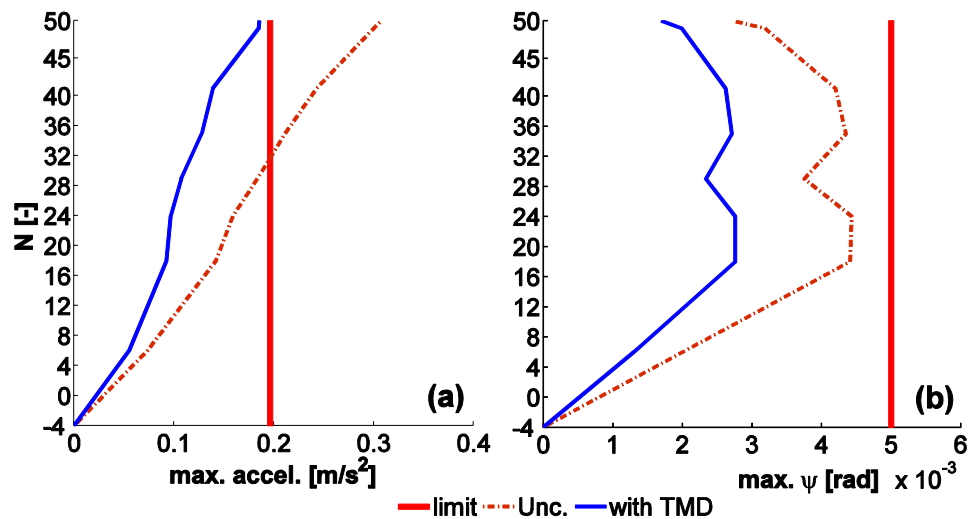


Fig. 11 All floors peak accelerations for a 10 years return period, and peak drifts for a 100 years return period in the x-direction, with and without the TMD

Table 2 lists the uncontrolled and controlled responses of the building in the x-direction under a wind direction of 292.5°. For safety concerns, mean wind speed that corresponds to a return of 100 years is used. RMS and peak values of the displacement at the top of the building, RMS and peak values of maximum inter-story drift, RMS and the peak values of shear loads (SL) at the ground level, and RMS and peak values of bending moment (BM) at the ground level are considered. Percentages of response reduction are indicated in the table (between brackets). Under wind loads with a return of 100 years, TMD can provide substantial reductions in the displacement and inter-story drift of the building. Design loads are reduced by about 20% to 46%.

4.4 Controlled response in the Y-direction

Fig. 12 shows the controlled and uncontrolled peak acceleration responses of the building in both x- and y-directions under wind loads with different direction angles. While the TMD can minimize the acceleration response in the x-direction to a value lower than the design criterion, the TMD in the y-direction is not effective. Fig. 12(b) shows that, under wind loads with a return of 10 years, a TMD with a mass ratio of 3% (inertial mass of TMD to the generalized mass of the building) is not able to reduce the acceleration response in terms of peak values lower than the maximum allowable values for two wind direction angles (0° and 292.5°). The TMD is capable of achieving response reduction over all the other wind direction angles. While uncertainty in the building's stiffness indicates that the TMD is robustly designed (to reduce STD accelerations), and the TMD can provide significant reductions in the STD and peak accelerations in both x- and y-directions for all the wind direction angles, the TMD in the y-direction requires heavier mass and is shown to be unable to achieve the comfort perception. For this reason a different control system will be considered in the y-direction.

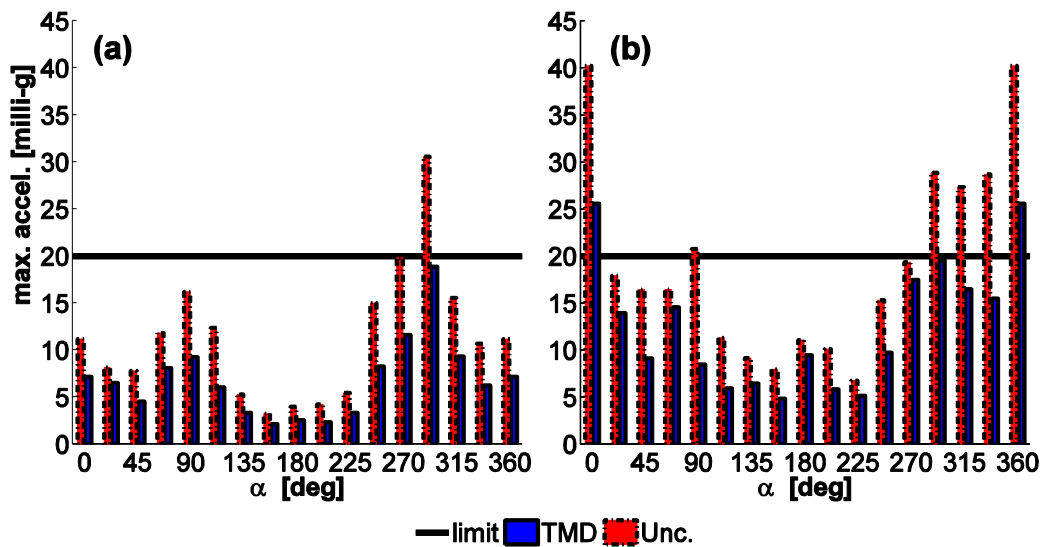


Fig. 12 Peak accelerations for a 10 years return: (a) x-direction, and (b) y-direction

5. Vibration control by MR dampers

5.1 MR damper configuration

Since the TMD was shown unable to reduce the acceleration response in the y-direction, lower than the criterion for serviceability and design, MR dampers as an alternative control system were considered. That is the case study building, which was successfully controlled in the x-direction by a TMD; it will be controlled in the y-direction with MR dampers creating a hybrid TM/MR damper control system for the whole building. While it is obvious for MR dampers to be connected between two points in a building, where significant drift exist, in tall buildings such requirement can be barely achieved. The challenge with high-rise buildings is that the drift between adjacent floors, especially in the y-direction, is not sufficient for a damper to work properly. This can be explained by considering the modal drifts, for example, between floors 16 and 21 in the diagonal direction, where a MR damper would be connected. As indicated by Fig. 3 and the values listed in Table 1, the diagonal drifts are relatively small. For this reason, a drift magnification mechanism is considered. The proposed drift magnification mechanism consists of a lever, pre-tensioned bracing, and a helical spring to create pre-tension (see Fig. 13). To allow for better energy dissipation, the MR damper was connected between ground and a point on the building via the drift magnification mechanism. The lever mechanism indicated in Fig. 13 is used for the purpose of displacement magnification across the damper. The magnification factor (MF) is defined as

$$MF = \frac{L_2}{L_1} = \frac{x_d}{x_f} = \frac{F_f}{F_d}, \quad > 1. \quad (19)$$

where L_1 and L_2 are arms of the lever; x_d is the displacement across the damper and

$$x_f = X_f \cos(\theta) \quad (20)$$

in which X_f is the drift between an arbitrary floor (where the bracing is connected) and ground, θ is the inclination angle of the bracing, F_f is force acting on the floor through the diagonal bracing and F_d is the force produced by the damper. Notice that for the lever to be effective, the length L_2 (building side) should be greater than L_1 (damper side), which means $MF > 1$. Not only can the proposed lever mechanism improve the performance of the MR dampers (as it increases the velocity across the damper and hence the amount of energy dissipated per cycle), but also it may reduce the required number of devices or allow to consider devices with lower damping capacity. However, this will increase control force in the bracing system, which means the need to have a stronger bracing link.

In modelling the damper bracing connection, to account for a realistic behavior of the system, the design of the bracing system is based on the assumption that the bracing members are circular steel bars with diameters that can be calculated according to the working allowable stress of the steel member.

For a certain allowable stress and a known bracing length, the corresponding bracing stiffness can be found using Hooke's law

$$E = \frac{\sigma_{all}}{\varepsilon} = \frac{F_{max} L_b}{A_b \delta} \quad (21)$$

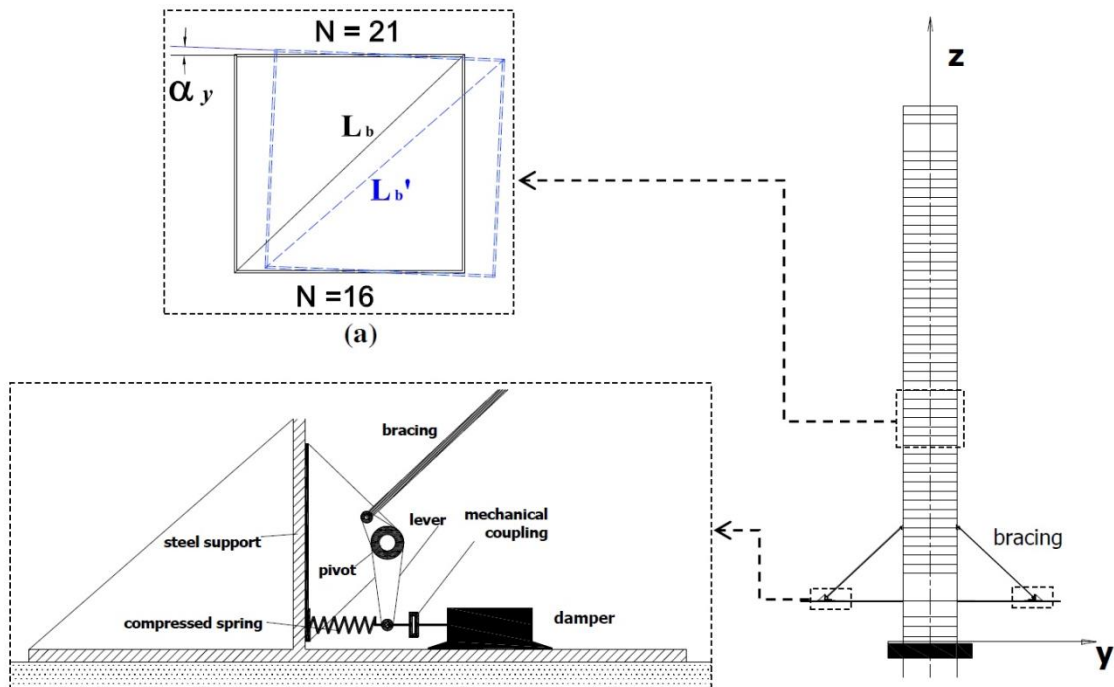


Fig. 13 MR dampers configuration in the y-direction: (a) challenging small inter-story drifts, (b) proposed damping unit, and (c) outer bracing

where E is the modulus of elasticity of the bracing material (about 209 GPa for steel), σ_{all} is the allowable working stress, ε is the corresponding strain, F_{max} is the maximum working force in the bracing member (including the pretension load), L_b is the bracing length, A_b is the cross-sectional area, and δ is the corresponding deflection. Eq. (21) gives the stiffness of the bracing as

$$k_b = \frac{F_{max}}{\delta} = \frac{E A_b}{L_b} = \left(\frac{E}{L_b} \right) \left(\frac{F_{max}}{\sigma_{all}} \right). \quad (22)$$

The deformation in the bracing element as a function of the working stress can be given by

$$\delta = \frac{\sigma_{all} L_b}{E} \quad (23)$$

For a realistic design, the bracing member is assumed to be able to carry a stress in the range of 40 MPa to 200 MPa as an overall working stress (including the pretension stress). The pretension load is assumed to be the same as the maximum capacity of the damper. Five different stiffness configurations are considered for allowable stresses of 40, 80, 120, 160, and 200 MPa.

5.2 Maxwell spring-damper model

Since the bracing is not completely rigid, the resulting assembly of the MR damper with the bracing will be similar to the Maxwell spring-damper model. The Maxwell element consists of spring and damper elements connected in series, as shown in Fig. 14. The element, massless and uni-axial, does not take into account the bending or torsion stiffness. The end points of the element can be attached to any bodies. The Maxwell element is suitable to model material responses that exhibit deformation under axial loads (Makris and Constantinou 1991). The corresponding equations, derived for the damper deflection, x_d , bracing deflection, x_b and the total deflection, x are

$$F_d = F_b = k_b x_b \quad (24)$$

$$x = x_d + x_b \quad (25)$$

Due to the fact that the MR damper is highly nonlinear, the analytical solution of the above equations is complex. The solution to these equations is conducted numerically in SIMULINK (Attaway 2009).

To control the response of the building in the y-direction, a number of MR dampers were considered. The single MR damper model has a maximum capacity of 1000 kN and mathematically modeled using the Bouc-Wen model (Yi *et al.* 1999). The equations governing the force, F_d , predicted by this model are as follows

$$F_d = c_0 \dot{x} + \alpha z \quad (26)$$

$$z = \gamma |\dot{x}| z |z|^{n-1} - \beta \dot{x} |z|^n + A \dot{x} \quad (27)$$

where z is the evolutionary variable that accounts for the history dependence of the response. The model parameters depend on the input voltage, v , to the current driver as follows

$$\alpha = \alpha_a + \alpha_b u; \quad c_0 = c_{0a} + c_{0b} u; \quad \dot{u} = -\eta(u - v) \tag{28}$$

The parameters of the MR damper were selected so that the device has a capacity of 1000 kN, as follows (Khajekaramodin *et al.* 2007): $\alpha_a = 1.0872e5$ N/cm, $\alpha_b = 4.9616 \times 10^5$ N/(cm.V), $c_{0a} = 4.4$ N.s/cm, $c_{0b} = 44$ N.s/(cm.V), $n = 1$, $A = 1.2$, $\gamma = 3$ cm⁻¹, $\beta = 3$ cm⁻¹, $\eta = 50$ s⁻¹. The model is simulated under a sine wave input with a frequency of 0.1 Hz (wind engineering applications) for different amplitudes (from 0.01 m to 0.1 m) for both 0 Volt and 10 Volt as indicated in Fig. 15.

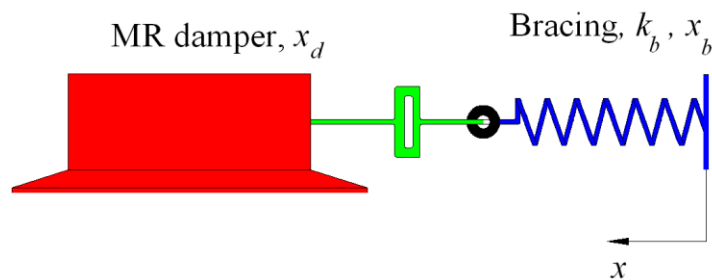


Fig. 14 Maxwell like model of the MR damper in contact with bracing

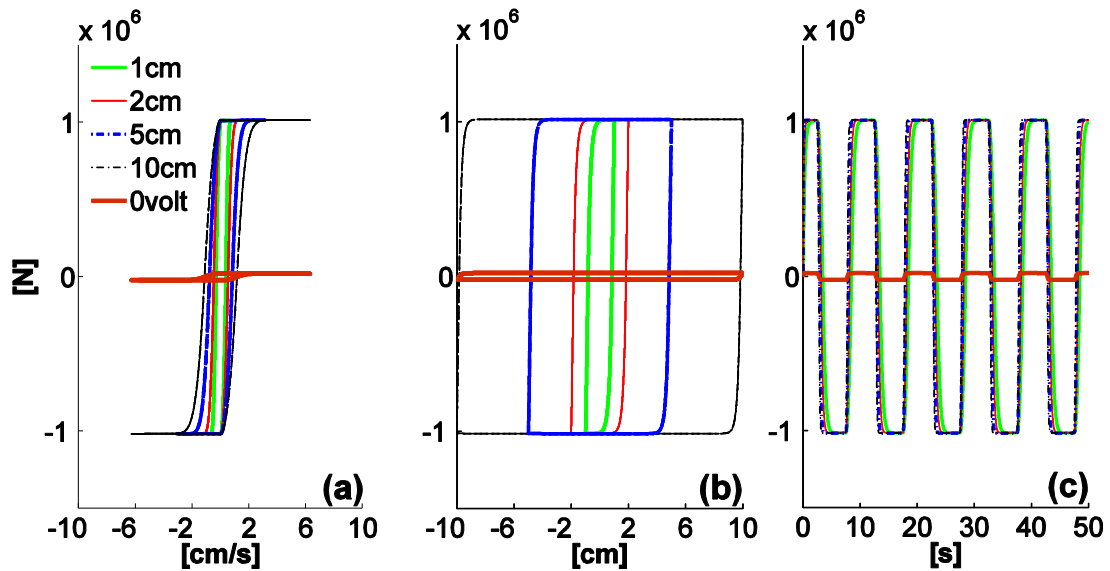


Fig. 15 Hysteresis loop of the MR damper under an input sinusoidal displacement with different amplitudes (1, 2, 5 and 10 cm) and an input voltage of 10 volt, and a sinusoidal displacement with 10 cm amplitude and 0 volt: (a) force versus velocity, (b) force versus displacement, and (c) force versus time

It is shown that the damper is able to provide the maximum damping force at a frequency of 0.1 Hz under different amplitudes of excitation. However, the amount of energy dissipated per cycle (the area enclosed in the hysteresis loop of the subfigure (b)) is increased by increasing the amplitude of the sine wave input. In practical applications, in order to increase the energy dissipated in one cycle, the velocity across the damper is to be increased. Velocity depends on the displacements amplitude and the frequency of oscillation. Since buildings oscillations under wind loads are characterized by low frequencies, one has to increase the displacement across the damper in order to increase the energy dissipated and hence improve efficiency.

A decentralized bang-bang controller is used with the MR dampers (Dyke and Spencer 1997, McClamroch and Gavin 1995). In this approach, the following control law is chosen

$$v_i = V_{\max} H(-\dot{\mathbf{x}}^T \mathbf{A} \mathbf{f}) \quad (29)$$

where v_i is the input voltage to the current driver of the i^{th} MR damper, and V_{\max} is the maximum allowable voltage and $H(\cdot)$ is the Heaviside step function. Notice that this control law requires only measurements of the floor velocities (only those in contact with the MR dampers), and the applied control forces.

5.3 Controlled response in the Y-direction

Four MR dampers are connected with a bracing-lever system between the ground and floor 6 (Fig. 13). This configuration as well as the number of dampers, and the magnification factor was achieved by trailing several options, with the objective of minimizing the bracing length, and at the same time creating significant drifts across the dampers. A magnification factor of 3 was used. The overall deflection in the bracing system is used as an indicator of the bracings stiffness. To examine the effect of the MR dampers on the responses of the building in the y-direction, a bracing system with an overall deflection of 15 mm is used (about 120 MPa working stress). The stiffness of the helical spring was selected to give permit sufficient pretension in the bracing member and was assumed to be constant. This is to allow the damper to work properly all the time (i.e. to provide damping whenever the floor is moving to the right or to the left). The responses of the controlled building, in the y-direction, under the wind direction of 0° were studied. The effect of the bracing stiffness was investigated by considering two cases (flexible and rigid), with a passive-on (constant input voltage to the current driver of the MR damper), and the decentralized control law mentioned previously. Fig. 16 shows the acceleration response for a 10 years return period and the drifts for a 100 years return period for the rigid and flexible bracing systems, for both the passive-on and the decentralized control cases, along with the original uncontrolled response. Fig. 16 indicates that both control systems are showing significant reductions in the responses of the building over the uncontrolled case. However, the decentralized controller is showing better performance with the realistic (flexible) bracing system. The ideal (rigid) bracing decreased the performance of the decentralized controller in reducing peak accelerations, which may be attributed to the shock created by the on-off control, when the bracing is rigid. Such effect is reduced with the flexible bracing (real case), as per delay in the application of the control force to the building. This may lead to an important conclusion, that is, the on-off control performance in reducing peak accelerations for a flexible bracing system is better than that with a rigid bracing system.

Table 3 gives the uncontrolled and controlled responses of the building in the y-direction. Under wind loads with a return period of 10 years, MR dampers with both passive-on (constant input voltage to the current drivers of the dampers) and decentralized bang-bang controller are able to bring the RMS and peak accelerations lower than the maximum allowable values, for the assumed uncertainty in the buildings stiffness, except for the “-10% stiffness” with the decentralized controller where the peak acceleration is slightly high. However, this may be accepted as the RMS accelerations are much lower than the maximum allowable value (5.7 milli-g). The decentralized bang-bang controller is performing better than the passive-on case in reducing RMS acceleration values for the building with stiffness uncertainties which indicates the robustness of this controller (see also Fig. 17).

The results listed in Table 3 also show that, under wind loads with a return period of 100 years, MR dampers with both passive-on and decentralized bang-bang controller are capable of significantly reducing the responses of the building in the range of 42.76% to 71.56%. Increasing the stiffness of the primary structure by 10% has no significant effect in the reduction in the peak foundation bending moment; it can increase the STD values of shear and bending moment at the foundation, in addition to no significant effect on the STD values of displacement. This reveals the importance of damping enhancement in tall buildings, as means by which the responses can be significantly reduced, with expected lower cost, compared to stiffness enhancement. The decentralized bang-bang controller is better than the passive-on in reducing all of the RMS responses. In addition, this controller is able to reduce the peak shear loads (SL) and the peak bending moment (BM) over the passive-on case. In any case, to permit the understanding of the semi-active control strategy, a dissipative analysis is carried out in the following section.

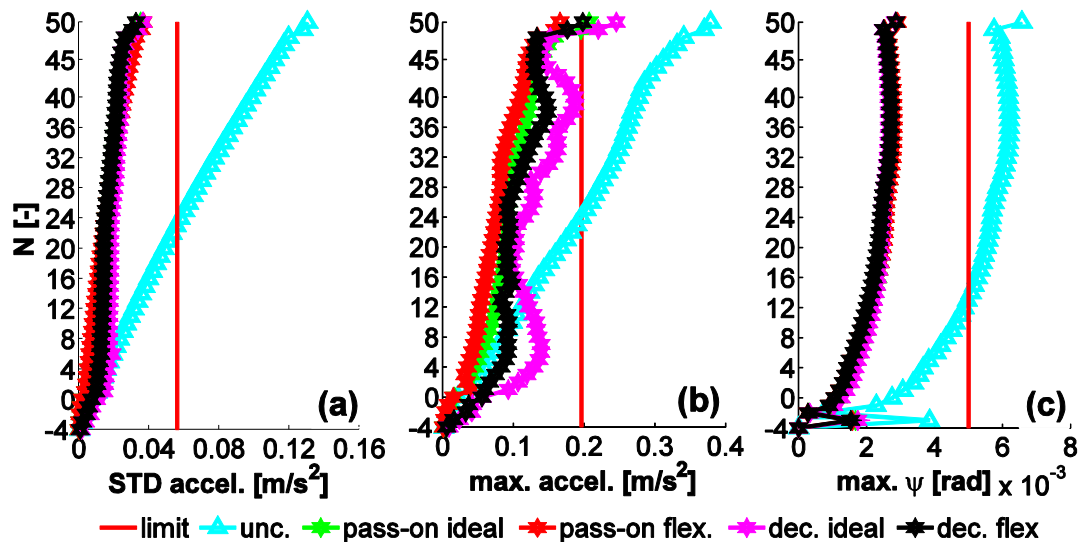


Fig. 16 Acceleration response for a 10 years return period and drifts for a 100 years return period

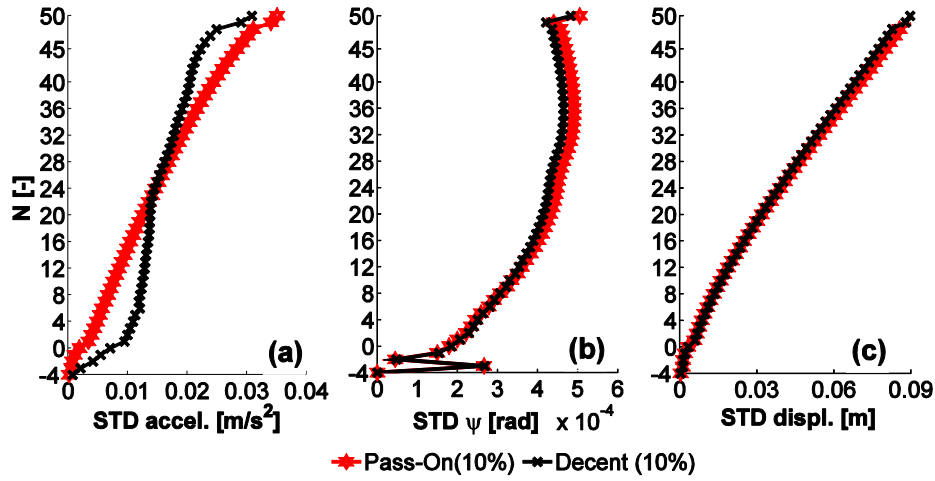


Fig. 17 Accelerations for a 10-years return period and drifts for a 100-years return period obtained with the decentralized and the passive-on control cases with the MR damper

Table 3 Buildings responses for both comfort and safety reasons (y-direction)

Criteria	Unc.	Passive-on		Decentralized bang-bang			
	+0% Stiffness	+0% Stiffness	+10% Stiffness	-10% Stiffness	+0% Stiffness	+10% Stiffness	-10% Stiffness
RMS Acc. (mg)	13.0268	3.6350 (72.10 %)	3.4710	3.8138	3.1292 (75.98 %)	2.9582	3.3362
I Peak Acc. (mg)	37.7087	16.1623 (57.14 %)	17.1560	18.4160	17.9946 (52.28 %)	16.1197	20.7541
RMS Disp. (m)	0.3496	0.1046 (70.08 %)	0.0929	0.1160	0.1001 (71.37 %)	0.0897	0.1116
II Peak Disp. (m)	1.2290	0.5381 (56.22 %)	0.4854	0.5637	0.5203 (57.66 %)	0.4989	0.5649
RMS Drift (rad)	0.0011	0.0006 (56.22 %)	0.0005	0.0006	0.0005 (71.58 %)	0.0005	0.0006
Peak Drift (rad)	0.0066	0.0029 (56.06 %)	0.0027	0.0031	0.0029 (56.06 %)	0.0027	0.0030
RMS SL (N)	1.347×10^7	4.711×10^6 (65.03 %)	4.521×10^6	4.80×10^6	4.415×10^6 (67.22 %)	4.273×10^6	4.513×10^6
Peak SL (N)	4.864×10^7	2.784×10^7 (42.76 %)	2.925×10^7	2.13×10^7	2.572×10^7 (47.11 %)	2.673×10^7	2.044×10^7
RMS BM (N.m)	1.994×10^9	6.538×10^8 (67.21 %)	6.231×10^8	6.69×10^8	6.055×10^8 (69.64 %)	5.803×10^8	6.234×10^8
Peak BM (N.m)	6.873×10^9	3.759×10^9 (45.31 %)	3.679×10^9	2.95×10^9	3.484×10^9 (49.32 %)	3.652×10^9	2.795×10^9

I: R = 10 yrs, U = 28 m/s; II: R = 100 yrs, U = 34 m/s

6. Dissipative analysis

This section is about the dissipative analysis of a simplified SDOF, representative of the case study building in one lateral direction. The idea behind the study of this system is to permit the understanding of the role of the dissipative and non-dissipative forces on this simplified model in a classical way. Accordingly, the classical SDOF system was represented as shown in Fig. 18(a). The application of a generic active control force, based on the classical control theory, will result in modifications to the structural stiffness and damping by the amounts k_a and c_a , respectively, as show in Fig. 18(b). The active control force can be dissipative or non-dissipative at any certain time. To better understand this, imagine the SDOF system in Fig. 18(b) is moving from its static equilibrium position 'O' towards the extreme right hand side position 'A'. During this time (part of a full cycle), the forces developed in the spring (k_a) and the damper (c_a) are dissipative (in the opposite direction of the motion). Since the active control force is proportional to two types of gains: velocity and displacement gains (k_a and c_a), this force is dissipative when the system is moving from its 'O' to 'A'. Now imagine the system is about to move from 'A' towards 'O', the spring force is at its maximum value, while the damper force is zero. The spring force will be in the same direction of the motion (non-dissipative) and the damper force will be in the opposite direction all time (dissipative). The damper force will increase from zero, at 'A', to a maximum value at 'O', while the spring force will decrease from its maximum value to a zero value at 'O'. This means that the total active control force (damper force + spring force) will change from non-dissipative to dissipative while the system is moving from 'A' to 'O'. if the control force is to be provided by a velocity gain only, the spring force will be zero all times, and the probability that the control force is dissipative is 1. On the opposite, if the control force is provided by a displacement gain only, the control force will be dissipative over a half of the cycle (from 'O' to 'A') and will be non-dissipative over the other half of the cycle (from 'A' to 'O') giving a probability of an active control force to be dissipative of 0.5. That is, any general control force with both velocity and displacement gains will have a probability of being dissipative with a value between 0.5 and 1. The probability that the active control force is dissipative can be expressed as a function of the properties of the primary structure (SDOF system) and the active control force (velocity and displacement gains) (Inaudi 2000, Aly and Christenson 2008, Erkus and Johnson 2011). Fig. 19 shows that at relatively low control forces, the probability that these forces are dissipative is very high (close to 1). It is also shown that higher control forces have relatively lower probabilities of being dissipative. This means that an optimum active controller based on the classical optimum control theory (see Soong 1990), will tend to modify the damping of the primary structure if the control forces are relatively low. On the other hand, an optimum active controller will tend to modify both rigidity and damping of the primary structure at relatively high control forces.

Fig. 19 shows that increasing the weight on the active control force will reduce the acceleration response significantly to some extent. After that the reduction will not be significant. Now imagine the same amount of force is to be provided by a viscous damper only. The viscous damper would tend to adapt only the damping of the system all the time (the dissipative probability is 1). Fig. 19 shows that the performance of the viscous damper (Viscous) is very similar to that of the active controller (Active) at relatively low control forces. At higher control forces the performance of the viscous damper will drop significantly.

Now let's think about an ideal semi-active control force. Imagine the semi-active damper is to be turned on and off based on the value of the corresponding active control force. This approach is

known as the clipped optimal control law (Dyke *et al.* 1996). Using the clipped optimal control law, the ideal semi-active control force at a certain time will be the same as the active control force, if the active control force is dissipative (smart damper turned on). When the active control force is non-dissipative, the ideal semi-active control force will be zero (smart damper turned off). This said, the semi-active control damper will only adapt the damping of the system for a fraction of time, while a viscous damper will adapt the damping all time. The active control force, however, adapts both damping and stiffness of the system all time. The performance of the semi-active system diverges from that of the active controller in the region corresponding to the decrease in the probability of dissipative forces as noted in previous studies by the author (Aly and Christenson 2008). In addition, the figure shows that at lower semi-active control forces (corresponding to the control forces produced by the MR dampers on the building in the y-direction), it is difficult to achieve much performance improvement over the passive-on case for this specific structure. However, at higher semi-active control forces the performance of the active and passive diverges and better performance over the passive-on case is expected.

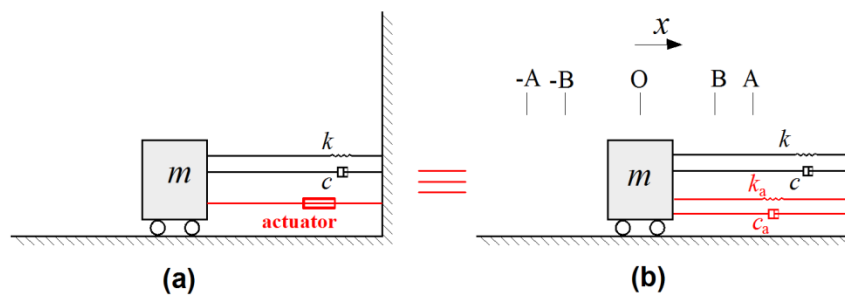


Fig. 18 SDOF system with the effects of control on the primary properties

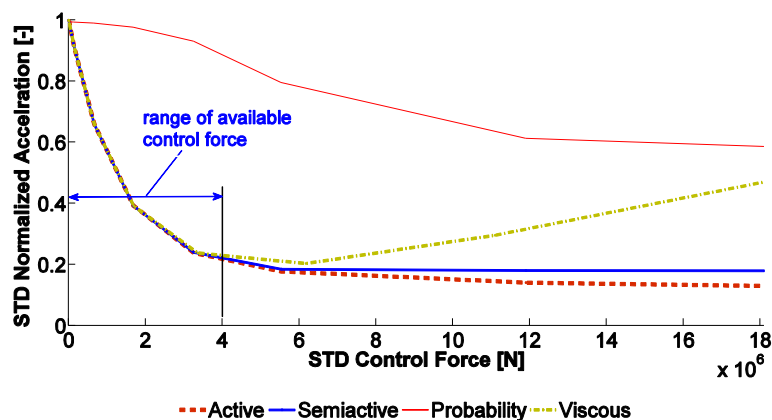


Fig. 19 Dissipative analysis of the SDOF system under active control forces: the vertical axis is representative of both the normalized acceleration and the probability of control forces being dissipative (Probability)

The dissipative analysis shows that high-rise buildings significantly lack damping and the best control method should focus on damping enhancement, rather than stiffness enhancement. An active controller tends to modify both damping and stiffness of the primary structure in an optimal way, based on an optimization objective. For instance, when the objective is to reduce the acceleration response, the active controller tends to first increase structural damping. This can be noticed in Fig. 19 as the probability of having dissipative forces is very close to 1. Unless aggressive actuators are used the control force is mostly dissipative by nature. Accordingly, viscous dampers (passive-on case) should provide noticeable performance, compared to active and semi-active control devices.

7. Conclusions

The purpose of this paper is to stimulate, shape, and communicate ideas with the state-of-the-art control technologies that are essential for solving wind related problems in high-rise buildings, with an objective to build the more resilient and sustainable constructions and to optimally retrofit existing ones. The paper presents a hybrid TM/MR dampers control system for a high-rise building under wind loads. The hybrid control system can reduce the building responses in the two lateral directions. The system has a robust TMD that was proposed for one lateral direction, and MR dampers in the other lateral direction, for a building with stiffness uncertainties to investigate the robustness of the control scheme. To show the applicability of the proposed control scheme, the TMD was attached to the top of the high-rise building, considering multidirectional wind loads. Due to the slenderness of the building in the other lateral direction, a passive TMD was not able to reduce the responses for serviceability design, with a reasonable mass ratio; accordingly, outer bracings with MR dampers were used. The main outcomes of the paper are summarized as follows:

1. The results show that increasing the stiffness of the building by 10%, 20%, and 50% did not show significant response reduction benefits. That is, stiffness increase in high-rise buildings may not be a feasible solution, and may not be used for the design for comfort and serviceability.
2. The paper presents a case study of an engineered design that is instructive. Basically, due to its geometry (unequal aspect ratios in the two lateral directions), with a heavy mass for the TMD in one lateral direction (very slender cantilever building), it was not possible to achieve the required response reduction, while two-thirds of the mass was sufficient in the other direction (shear building). This may lead to the conclusion that high-rise buildings can behave differently under same wind conditions, as per their shape and orientation, among other factors, and a certain control system that is optimal for a building may not be suitable for another.
3. Comparisons of the controlled and uncontrolled responses demonstrate the effectiveness of the proposed control system. The performance of the TMD is remarkable in reducing the responses of the high-rise buildings under real wind loads. Although the objective of the application of the TMD was to reduce accelerations for comfort reasons, the wind-induced loads are also reduced, which may improve the resiliency of the main structure.

4. The use of lever mechanism and outer bracing offers an attractive way to control high-rise buildings. For a cantilever-like behaving structures, outer MR damper-bracing with lever mechanisms for motion magnification is an excellent alternative to TMDs.
5. The on-off control performance in reducing peak accelerations with a flexible bracing system is better than that with a rigid bracing system. The ideal (rigid) bracing decreased the performance of the decentralized controller in reducing peak accelerations, which may be attributed to the shocks created by the on-off control forces, when the bracing was assumed rigid.
6. For the purpose of using MR dampers, an on-off control of the devices may enhance their performance, compared with the passive-on case.
7. High-rise buildings have inherently low damping, which makes the priority of a control system to increase damping rather than stiffness modification. This was better explained by the dissipative analysis carried out in the current paper. The dissipative analysis shows that the decentralized control algorithm, commanding the MR dampers, is working within the possible range of optimum performance.

Disclaimer

The opinions expressed in this paper are those of the author and do not necessarily reflect the views of any institution/firm.

References

- Aly, A.M. (2013), "Pressure integration technique for predicting wind-induced response in high-rise buildings", *Alexandria Eng. J.*, **52**(4), 717-731.
- Aly, A.M. (2009), *On the dynamics of buildings under winds and earthquakes: response prediction and reduction*, Diss. Ph. D. thesis, Department of Mechanical Engineering, Politecnico di Milano, Milan, Italy.
- Aly, A.M., Zasso, A. and Resta, F. (2011a), "On the dynamics of a very slender building under winds: Response reduction using MR dampers with lever mechanism", *Struct. Des. Tall Spec. Build.*, **20**(5), 539-551.
- Aly, A.M. (2014), "Proposed robust tuned mass damper for response mitigation in buildings exposed to multidirectional wind", *Struct. Des. Tall Spec. Build.*, **23**(9), 664-691.
- Aly, A.M. and Christenson, R.E. (2008), "On the evaluation of the efficacy of a smart damper: a new equivalent energy-based probabilistic approach", *Smart Mater. Struct.*, **17**(4), Article ID 045008.
- Anthony, W.R. and Stainer, P.J. (1988), "Concrete high rises offer many cost advantages", *Concrete Constr.*, **33**(5), 453-456.
- Attaway, S. (2009), *Matlab: A Practical Introduction to Programming and Problem Solving*, Butterworth-Heinemann, Amsterdam, Netherlands.
- Bendat, J.S. and Piersol, A.G. (2000), *Random Data Analysis and Measurement Procedures*, 3rd Ed., Wiley Series in Probability and Statistics, New York, USA.
- Chowdhury, I. and Dasgupta, S. (2003), "Computation of rayleigh damping coefficients for large systems", *Electronic J. Geotech. Eng.*, **8**, Bundle 8C.
- Clinton, J.F., Bradford, C.S., Heaton, T.H. and Favela, J. (2006), "The observed wander of the natural frequencies in a structure", *Bull Seismol. Soc. Am.*, **96**(1), 237-257.
- Goncalves, F.D., Koo, J.H. and Ahmadian, M. (2006), "A review of the state of the art in magnetorheological fluid technologies—part I: MR fluid and MR fluid models", *Shock Vib. Digest*, **38**(3),

- 203-219.
- CTBUH (2015), "CTBUH tall buildings database", Council on Tall Buildings and Urban Habitat (CTBUH), <http://www.skyscrapercenter.com/buildings>, retrieved on May 31, 2015.
- Dyke, S.J., Spencer, B.F., Sain, M.K. and Carlson, J.D. (1996), "Modeling and control of magnetorheological dampers for seismic response reduction", *Smart Mater. Struct.*, **5**(5), 565-575. DOI: 10.1088/0964-1726/5/5/006.
- Dyke, S.J. and Spencer, B.F. (1997), "A comparison of semi-active control strategies for the MR damper", *Proceedings of the 1997 IASTED International Conference on Intelligent Information Systems (IIS '97)*, Grand Bahama Island, BAHAMAS, December 08-10, 1997. DOI: ieeecomputersociety.org/10.1109/IIS.1997.645424.
- Erkus, B. and Johnson, E.A. (2011), "Dissipativity analysis of the base isolated benchmark structure with magnetorheological fluid dampers", *Smart Mater. Struct.*, **20**, Article ID 105001.
- Eurocode 1. (2004), Eurocode 1: Actions on structures — General actions — Part 1-4: Wind actions. prEN 1991-1-4: European Standard.
- Feng, M.Q. and Mita, A. (1995), "Vibration control of tall buildings using mega subconfiguration", *J. Eng. Mech - ASCE*, **121**(10), 1082-1088.
- Ghorbani-Tanha, A.K., Noorzad, A. and Rahimian, M. (2009), "Mitigation of wind-induced motion of Milad tower by tuned mass damper", *Struct. Des. Tall Spec. Build.*, **18**, 371-385. Doi: 10.1002/tal.421
- Gu, M. and Peng, F.J. (2002), "An experimental study of active control of wind-induced vibration of super-tall buildings", *J. Wind Eng. and Ind. Aerod.*, **90**(12-15), 1919-1931.
- Gur, S., Mishra, S.K., Bhowmick, S. and Chakraborty, S. (2014), "Compliant liquid column damper modified by shape memory alloy device for seismic vibration control", *Smart Mater. Struct.*, **23**(10), 105009.
- Halsey, T.C. (1992), "Electrorheological fluids", *Science*, **258**(5083), 761-766.
- Hart, G.C., Jain, A. and Ekwueme, C.G. (2010), "Smart buildings: viscous dampers", *Struct. Des. Tall Spec. Build.*, **19**(4), 373-396.
- Housner, G.W., Bergman, L.A., Caughey, T.K., Chassiakos, A.G., Claus, R.O., Masri, S.F., Skelton, R.E., Soong, T.T., Spencer, B.F. and Yao, J.T.P. (1997), "Structural control: Past, present, and future", *J. Eng. Mech. - ASCE*, **123**(9), 897-971.
- Irwin, P., Kilpatrick, J., Robinson, J. and Frisque, A. (2008), "Wind and tall buildings: negatives and positives", *Struct. Des. Tall Spec. Build.*, **17**(5), 915-928.
- Inaudi, J.A. (2000), "Performance of variable-damping systems: theoretical analysis and simulation", *Proceedings of the 3rd International Workshop on Structural Control*, Paris, France, July 6-8.
- Jin, X., Zhang, G., Zuo, J. and Lindsay, S. (2013), Sustainable high-rise design trends-Dubai's strategy", *Civil Eng. Architect.*, **1**(2), 33-41.
- Khayrullina, A., van Hooff, T. and Blocken, B. (2013), "A study on the wind energy potential in passages between parallel buildings", *Proceedings of the 6th European and African Conference on Wind Engineering*, Robinson Cambridge, United Kingdom, July.
- Kim, D.H., Ju, Y.K., Kim, M.H. and Kim, S.D. (2014), "Wind-induced vibration control of tall buildings using hybrid buckling-restrained braces", *Struct. Des. Tall Spec. Build.*, **23**(7), 549-562.
- Lee, J.J. and Yun, C.B. (2006), "Damage diagnosis of steel girder bridges using ambient vibration data", *Eng. Struct.*, **28**(6), 912-925.
- Leitmann, G. (1994), "Semiactive control for vibration attenuation", *J. Intell. Mat. Syst. Str.*, **5**, 841-846.
- Li, C., Li, J. and Qu, J. (2010), "An optimum design methodology of active tuned mass damper for asymmetric structures", *Mech. Syst. Signal Pr.*, **24**(3), 746-765.
- Li, Q.S., Yang, K., Zhang, N., Wong, C.K. and Jeary, A.P. (2002), "Field measurement of amplitude dependent damping in a 79-storey tall building and its effects on the structural dynamic responses", *Struct. Des. Tall Build.*, **11**, 129-153.
- Liu, C. and DeWolf, J.T. (2007), "Effect of temperature on modal variability of a curved concrete bridge under ambient loads", *J. Struct. Eng. - ASCE*, **133**(12), 1742-1751.
- Lu, X., Li, P., Guo, X., Shi, W. and Liu, J. (2012), "Vibration control using ATMD and site measurements on

- the Shanghai World Financial Center Tower”, *Struct. Des. Tall Spec. Build.*, **23**(2), 105-123.
- Khajekaramodin, A., Haji-kazemi, H., Rowhanimanesh, A. and Akbarzadeh, M.R. (2007), “Semi-active control of structures using neuro-inverse model of MR dampers”, *Proceeding of the 1st Joint Congress on Fuzzy and Intelligent Systems*, Ferdowsi University of Mashhad, Iran 29-31 Aug.
- Makris, N. and Constantinou, M.C. (1991), “Fractional derivative model for viscous dampers”, *J. Struct. Eng. - ASCE*, **117**(9), 2708-2724.
- McClamroch, N.H. and Gavin, H.P. (1995), “Closed loop structural control using electrorheological dampers”, *Proceedings of the American Control Conference*, Seattle, Washington.
- Meirovitch, L. (1967), *Analytical Methods in Vibrations*, The Macmillan Co., New York.
- Metwally, H.M., El-Souhily, B.M. and Aly, A. (2006), “Reducing vibration effects on buildings due to earthquake using magneto-rheological dampers”, *Alex. Eng. J.*, **45**(2), 131-140.
- Midas (2015), Midas/Gen, http://www.cspfea.net/midas_gen.html
- Park, K.S. and Ok, S.Y. (2015), “Optimal design of hybrid control system for new and old neighboring buildings”, *J. Sound Vib.*, **336**, 16-31.
- Pelli, C., Thornton, C. and Joseph, L. (1997), *The World's Tallest Buildings*, Scientific American, 277, 92-101.
- Rosa, L., Tomasini, G., Zasso, A. And Aly, A.M. (2012), “Wind-induced dynamics and loads in a prismatic slender building: a modal approach based on unsteady pressure measurements”, *J. Wind Eng. Ind. Aerod.*, **107-108**, 118-130
- Satake, N., Suda, K., Arakawa, T., Sasaki, A. and Tamura, Y. (2003), “Damping evaluation using full-scale data of building in Japan”, *J. Struct. Eng. - ASCE*, **129**, 470-477.
- Simiu, E. and Scanlan, R. (1996), *Wind Effects on Structures*, John Wiley & Sons, New York.
- Smith R.J. and Willford, M.R. (2007), “The damped outrigger concept for tall buildings”, *Struct. Des. Tall Spec. Build.*, **16**(4), 501-517.
- Soong, T.T. (1990), *Active Structural Control: Theory and Practice*, John Wiley & Sons Inc.
- Spencer, B.F., Dyke, S.J. and Deoskar, H.S. (1998), “Benchmark problems in structural control. I: Active mass driver system, and II: Active tendon system”, *Earthq. Eng. Struct. D.*, **27**(11), 1127-1147.
- Tamura, Y. and Yoshida, A. (2008), “Amplitude dependency of damping in buildings”, *Proceedings of the 18th Analysis and Computation Specialty Conference*, Vancouver, Canada.
- Taylor, D. (2010), “Smart buildings and viscous dampers—a design engineer’s perspective”, *Struct. Des. Tall Spec. Build.*, **19**(4), 369-372.
- Yi, F., Dyke, S.J., Caicedo, J.M. and Carlson, J.D. (1999), “Seismic response control using smart dampers”, *Proceedings of the 1999 American Control Conference (99ACC)*, IEEE, San Diego, CA, USA, June 2- 4, 1999. DOI: [iel5/6343/16963/00783195](https://doi.org/10.1109/99.83195).
- Yuen, K.V. and Kuok, S.C. (2010b), “Modeling of environmental influence in structural health assessment for reinforced concrete buildings”, *Earthq. Eng. Eng. Vib.*, **9**(2), 295-306.
- Yuen, K.V. and Kuok, S.C. (2010a), “Ambient interference in long-term monitoring of buildings”, *Eng. Struct.*, **32**(8), 2379-2386.